SAND2018-2540J

Open Data, Models, and Codes for Redox Flow Batteries

Seong Beom Lee,[a,1] Harry D. Pratt III,[b,1] Travis M. Anderson,[b,1] Venkatasailanathan Ramadesigan, [c, 2] Kishalay Mitra,[d] Babu R. Chalamala,[b,2], and Venkat R. Subramanian [a, e,2,3]

[a] Department of Chemical Engineering, University of Washington, Seattle, WA 98195, USA
[b] Sandia National Laboratories, Albuquerque, NM 87185, USA
[c] Department of Energy Science and Engineering, Indian Institute of Technology Bombay, Powai, Mumbai, Maharashtra 400076, India
[d] Department of Chemical Engineering, Indian Institute of Technology Hyderabad, Kandi, Sangareddy, Telangana 502285, INDIA
[e] Pacific Northwest National Laboratory, Richland, WA 99354, USA

Abstract

Mathematical models of Redox Flow Batteries (RFBs) can be used to analyze cell performance, optimize battery operation, and control the energy storage system efficiently. Among many other models, physics-based electrochemical models are capable of predicting internal states of the battery, such as temperature, state-of-charge, and ions' concentration at positive and negative electrolytes. In the models, estimating parameters is an important step that can study, analyze, and validate the models using experimental data. A common practice is to obtain these parameters either through conducting experiments or from the information available in the literature. However, it is not easy to investigate all proper parameters for the models through this way, and there are occasions when important information, such as diffusion coefficients and rate constants of ions, is not readily available. The parameters needed for simulating charge-discharge performance are not always available. In this paper, an efficient way to estimate parameters of RFB using physics-based battery models has been proposed. Open source codes and executable files are provided as well, enabling to identify the performance of redox batteries without the need for software installation and a priori programming knowledge. This paper also demonstrates that the proposed approach can be used to study and analyze the aspects of capacity loss/fade, kinetics, and transport phenomena of the RFB system.

Keywords: Laboratory-scale static cell, Parameter estimation, Optimization, Vanadium redox static batteries, Capacity Fade/Loss, Open source codes and executable files

---

[1] Electrochemical Society Student Member
[2] Electrochemical Society Active Member
[3] Corresponding Author, Tel: +1-206-543-2271; Fax: +1-206-543-3778
Email: vsubram@uw.edu

Introduction

Redox Flow Batteries (RFBs) are promising energy storage systems for grid/microgrid applications.[1] There has been significant technological progress in the recent past towards meeting the growing need for large-scale energy storage systems such as RFBs.[2] Among different types of RFBs, Vanadium Redox Flow Batteries (VRFBs) have gained more attention, and as a result several physics-based electrochemical models for these systems describing the battery operations have been developed.[3-12]

Physics-based electrochemical models can be classified by dimensions, from zero- to two-dimensional models as shown in Table I. Models in each category have their own advantages and can be used depending on users' needs. For example, zero-dimensional models have been developed to be easily implementable, enabling to quickly understand, predict, and control the battery system.[9, 13] Multi-dimensional models have been implemented by including more detailed physics of the system.[3] As described in Table I, the current trend is to include detailed physical phenomena, such as transport of ions and side reactions of the system,[8, 12] and therefore models with more complexities have been built. Most models are still based on isothermal effects and dilute solution theory. A zero-dimensional model was developed for static cell systems including diffusion of vanadium ions through the membrane,[11] and this was the first attempt of to simulate ion crossover through the membrane.[11] The model was further developed to include all ions and transport properties of the system.[3, 13] One-dimensional membrane models based on dilute and concentrated solution theories have been developed assuming bulk electrolytes at positive and negative.[14, 15] Flow cell models have been developed in two-dimensions to include diffusion, migration, and convection of all ions and detailed physics of the system.[3]

An efficient way of combining physics-based electrochemical models and parameters estimation techniques can facilitate the research on large scale energy storage technologies which are indispensable for the success and growth of intermittent sources of energy. For instance, the current practice in the grid/microgrid control systems is to utilize empirical battery models regardless of the type of the batteries.[16] Extended battery life and reduction in the size of RFBs, which are two of the most critical factors in battery control system, can be achieved better if these empirical battery models are replaced with physics-based electrochemical models. The physics-based models have the power of predicting the battery performance and

internal states accurately. With such detailed models, an efficient equation-based PV-Battery microgrid framework was recently developed to be able to simulate the entire microgrid components including physics-based battery models in real-time, and the framework can implement any kind of physics-based electrochemical battery models.[17] Once the specific battery models are incorporated into the efficient equation-based microgrid framework, an important task is to estimate the parameters used in the model. The values of these parameters need updating at regular intervals to reflect the change in battery behavior over the cycles of charging/discharging. This enables the models to have accurate predictions for several states of battery parameters, leading to a better prediction of battery usability, life and improved safety. It also helps analyze and study the kinetics, transport phenomena, and capacity fade/ degradation of the flow cell. However, several attempts to estimate the states and parameters of VRFB system have been made using empirical/ equivalent circuit-based models, which do not include detailed physics of the battery.[18-20] Also, other research works on model development collect most of the parameters from experimental literature and only estimate one or two remaining parameters using mathematical models.[3, 9] However, many of these experiments require either physical destruction of the battery or tedious as well as sophisticated experimental setup.[21-23] For example, dialysis cell, pumps, and measuring cylinders are utilized to investigate diffusion coefficients of ions through a membrane in an RFB experimental setup.[24] Techniques like linear sweep voltammetry and electrochemical impedance spectroscopy were used to investigate reaction rate information for the kinetic parameters at electrodes.[25, 26]

The main objective of this paper is to open experimental data, models, and codes for parameter estimation of redox flow batteries. Open source codes and executable files, which can give a practical impact in a field of the battery research, are provided so that users can identify the performance of their batteries without any type of software installation and programming skills. In this paper, an efficient parameter estimation approach is also proposed, and we show that the proposed estimation approach can help study and analyze important aspects of batteries, such as capacity fade/loss, kinetics, and transport of ions, including physics-based battery models for a laboratory-scale static cell system. The laboratory-scale static cell system, consisting of a transparent H-cell, a membrane, electrolytes, and electrodes, has been used to study the performance of RFBs quickly due to its straightforward and easy implementation.[27] Estimation of all parameters of the physics-based electrochemical model for

Vanadium Redox Static Batteries (VRSBs) has been addressed using two cell systems, which include two different membranes, assuming that both systems have some common characteristics, such as kinetics at the electrodes, the formal potential, and the contact resistance except for diffusivity of ions through the membranes. First, a reference Nafion 115 membrane is used. As diffusion coefficients of vanadium ions for a Nafion 115 membrane are available in the literature, this information is utilized to estimate other cell system parameters, such as cell resistance and rate constants in the static cell model. The effects of diffusion and migration of ions in the system, which cause capacity fade/loss to the battery, have been analyzed based on the obtained information. Moreover, it has been shown that diffusion coefficients of vanadium ions for other membranes can be estimated based on the parameters estimated using the Nafion 115 system. Using this concept, four vanadium ions' diffusion coefficients of a Nafion XL membrane, which are not available in the literature, have been estimated. Once the parameters have been obtained, one can use the kinetic and transport parameters for simulating redox battery system as well.

Experimental

Materials. Vanadium (IV) oxide sulfate hydrate ($VOSO_4 \cdot xH_2O$)[28] and an aqueous sulfuric acid solution (H_2SO_4)[29] were purchased from Aldrich and used as received. Nafion XL[30] and Nafion 115[31] membranes were purchased from DuPont and used after pretreatment using distilled deionized water (DDW) and an aqueous sulfuric acid solution at 80°C for 30 minutes, respectively. POCO graphite electrodes were purchased from Saturn Industries.[32]

Instrumentation. The performance of the static cell was obtained at different C-rates, using a Solartron SI 1287 potentiostat.[33]

The static cell system. The H-cell (Adams and Chittenden Scientific Glass)[34] consists of a positive and a negative chamber as shown in Figure 1. A membrane is located between these two chambers and the membrane is in contact with the electrolytes of the half-cell. The volume of the electrolytes at the positive and the negative chamber is 10 ml each. Two graphite electrodes with specific reaction surface (1cm × 1cm × 0.1cm) are vertically placed in the center of each chamber and fixed with the plastic caps of the H-cell. There are rubber gaskets inside these plastic caps and silicon is attached to the gaps between the electrode and the gasket to prevent oxygen leakages from outside the system.

Preparation of electrolytes. Sulfuric acid solution (H_2SO_4, 6.73 ml) was slowly added to 7.5 ml of DDW, and the final volume was adjusted to 30 mL using DDW to prepare 4M sulfuric acid solution (H_2SO_4). 0.489g of vanadium (IV) oxide sulfate hydrate ($VOSO_4 \cdot xH_2O$) was added very slowly and stirred at 60°C for 1 hour. 30 mL of 0.1M vanadium (IV) oxide sulfate ($VOSO_4$) in an aqueous 4M sulfuric acid solution (H_2SO_4) was prepared. Next, 10 mL of 0.1M vanadium (IV) oxide sulfate ($VOSO_4$) in an aqueous 4M sulfuric acid solution (H_2SO_4) was added to the positive and negative chamber, respectively. The static cell system with Nafion 115 membrane was slowly charged at C/20 rate to convert VO^{2+} to V^{3+} at the anode and VO^{2+} to VO_2^+ at the cathode. When the upper limit voltage of 1.7V was exceeded, the charge was set to be terminated, and 93.9% V^{3+}/6.1% VO^{2+} electrolytes at the negative chamber were achieved by the coulombic calculation. VO^{2+}/VO_2^+ electrolytes at the positive chamber were drained and refilled with a new 10 mL of 0.1 M VO^{2+} in 4 M sulfuric acid solution (H_2SO_4) to achieve full state of charge of the static cell.

Cell operation. For the Nafion 115 system**,** a typical CC-CV profile (CC: Constant Current, CV: Constant Voltage) was applied (maximum voltage: 1.7V). Once the static cell voltage reached 1.7V, it was charged with the CV until the applied current is saturated. For discharging, a CC profile was applied. The CC-CV profile was used to analyze the cell systems' performance at different C-rates (C/20 and C/30), making the cell to reach full capacity and study the effects of diffusion and migration. For the Nafion XL cell system, we focused on parameter estimation on diffusion coefficients of the membrane, assuming that all cell system parameters are the same with the Nafion 115 system except for the ions' diffusion distance, the potential gradient inside the membrane, and diffusion coefficients through the membrane. For charging and discharging, therefore, a CC profile (C/30) was applied to the static cell system. The temperature of the H-cell was maintained at 25°C in a Tenney Environmental Chamber.[35] The gas washer, which was filled with water and connected to the argon line and cell system, minimizes evaporation of electrolytes. During the charging and discharging process, a magnetic stirrer was used to make uniform concentrations of the electrolyte in the positive and negative chambers.

Model

Coupling the static cell with zero-dimensional models enables easy and straightforward implementation and mitigates computational challenges to simulate models and estimate their

parameters. For this reason, a zero-dimensional model was implemented as an example for combining with the proposed estimation approach. Migration effects of vanadium ions through the membrane, the diffusion distance of the membrane, and kinetics at electrodes have been added[3, 9, 13] to a zero-dimensional electrochemical static cell model (demonstrated by Tang *et. al*[11]) which includes diffusion of vanadium ions through the membrane. Parameter estimation techniques were combined with the zero-dimensional model to estimate the parameters appearing in the equations. All relevant equations (Equations 1-4, 9-12, and 17-21 in Table II, III, IV, respectively), variables (Table V), and parameters (Table VI), which were used to model and simulate the VRSB system, are listed in Tables II-VI.[3, 9, 11, 13]

Assumptions. The following assumptions were made in the static cell model: (i) Side reactions between two different vanadium ions, due to diffusion and migration of ions through the membrane, occur immediately once vanadium ions cross the membrane;[3] (ii) Since the gas washer is connected to the static cell system to minimize evaporation of the electrolyte, evaporation of the electrolyte is ignored in the model; (iii) Faraday's law of electrolysis has been utilized to estimate the rate of reactions of vanadium ions at the cathode and anode; (iv) Hydrogen and oxygen that evolve at the electrode during charging and discharging, are ignored due to low C-rates;[8, 12] (v) Nafion 115 and Nafion XL systems have identical kinetics at the electrodes, the formal potential, and the contact resistance; (vi) The potential gradient inside a membrane remains constant during battery operation (charging and discharging); (vii) No side reactions take place between other vanadium ions in a membrane.

Diffusion and migration. The undesired but unavoidable crossover of vanadium ions through the membrane, which leads to capacity loss/fade during charging and discharging, is caused by the diffusion, migration, and convection of ions.[3] In this static cell model, however, diffusion and migration are considered as the main causes of transport. Convection is one of the important transport phenomena in flow cells, but not relevant in static cells since they contain static electrolytes. The diffusion of vanadium ions occurs at all times regardless of the cell's operating conditions since the driving force of the transport is the concentration gradient between the positive and negative electrolytes.[11] In contrast, the net flux of ions through the membrane by migration occurs differently. This is because the driving force of the crossover of ions is to maintain electrical neutrality of the positive and negative electrolytes. When vanadium ions cross the membrane, the ions face the potential gradient by migration effects,

which slows down or increases the total ion flux as shown in Figure 2. The migration effect occurs from the positive side to the negative side during charging, which is the same direction to the diffusion flux of VO^{2+} and VO_2^+ and the opposite direction to the diffusion flux of V^{2+} and V^{3+}. During discharging, the migration effect occurs from the negative side to the positive side for vanadium ions of the system. In the proposed model, both uni- and anti- directional migration effects (to the diffusion flux) inside a membrane have been added, assuming that the potential gradient of migration effects remains constant during charging and discharging. After that, the potential gradient is estimated directly. Also, the crossover of the vanadium ions through the membrane causes side reactions in the electrolyte as shown in Figure 3.[11] Once vanadium ions cross the membrane, reactions between two different vanadium ions occur, producing VO^{2+} ions at the positive electrolyte and V^{3+} ions at the negative electrolyte, and this, in turn, causes the capacity loss/fade of the battery.[11]

Governing equations. Equations 1-4 and 9-12 of the static cell model, as given in Tables II and III, depict the dynamics of the concentration of vanadium ions including diffusion and migration through the membrane during charging and discharging, respectively.[11, 13] This is a system of eight Ordinary Differential Equations (ODEs). In Tables II and III, mass balance equations, consisting of the rate of accumulation of ions, the rate of ions entering the opposite chamber, the rate of ions flowing out from their own chamber, and the rate of loss or generation of ions, were established for vanadium ions. In other words, the rate of accumulation of each vanadium ion species (V^{2+}, V^{3+}, VO^{2+}, and VO_2^+) is the sum of the rate of production of the vanadium ions by side reactions, the rate of outflow into the opposite chamber, and the rate of generation or loss at the electrode by the electrochemical reactions.[36]

Additional equations. Table IV presents additional equations including the cell voltage, the open circuit voltage, and the overpotential used in the model.[9, 11, 13] The cell voltage given by Equation 17 is used in the static cell model.[11] The formal potential is used to calculate open circuit voltage of the static cell system as given in Equation 18. To use the formal potential, the proton concentration is removed from the logarithmic term in the Nernst Equations.[11] The concentration of hydrogen ions in the positive half-cell electrolyte is not known accurately since several ionic equilibria affect the equilibrium concentrations of all the ionic species in the VRSB electrolyte.[11] The overpotential at the positive and negative electrodes, including the activation barrier, is calculated as given in Equation 19 and 20, and a charge transfer coefficient

of 0.5 is applied to the overpotential.[9] Equations 21 represents the conductivity of the membrane.[37]

Parameter Estimation

The model parameters are fitted with the experimental data to estimate their values using mathematical optimization techniques. There are ten parameters in the model, which are estimated by the parameter estimation approach, e.g., diffusion coefficients of four different vanadium ionic species for membranes, the contact resistance of the cell, two reference rate constants at cathode and anode, the formal potential, the diffusion distance of the membrane, and the potential gradient inside the membrane. Given certain realistic values of these parameters, the model can be simulated to predict the values of voltage at certain time intervals. The final estimated parameters are obtained by solving an optimization problem where the sum of squares of the differences in the voltage outputs between the model and experiment divided by the total number of experimental data points (known as the Mean Square Error, MSE) for the first cycle (charging and discharging) of the system is minimized, and unknown parameters are used as decision variables.[38] The objective function of the optimization approach can be expressed as follows:

$$\min \frac{1}{N} \sum_{j=1}^{N} [V_{exp,j} - V_{model,j}]^2 \qquad [22]$$

where N is the total number of experimental data points for charging and discharging, $V_{exp,j}$ and $V_{model,j}$ indicate the experimental and model predicted voltage value of the static cell for the j^{th} data point, respectively. In this paper, 200 data points for charge and discharge voltage was collected at regular time intervals. The optimization routine uses several values of the optimizing parameters iteratively before choosing the optimal values for which the objective function (as given in equation 22) subject to model equations, initial conditions, and bounds for the parameters, is minimized. The parameter estimation of ten parameters is performed with two cell systems. In each of the system, some parameters are known a priori while other parameters are estimated through the parameter estimation approach as shown in Figure 4. The initial guesses, bounds, converged parameters, and minimized MSE are summarized in Table VII, and the values in Table VII were rounded off to the fifth decimal place (original values are

presented in text files of open source codes). Analyses and studies of simulations and optimizations in this work were carried out on a workstation with dual 8-core, 3.10GHz Intel Xeon processors, 32.0 GB RAM using the NLPsolve (optimization method: nonlinearsimplex, and evaluation limit: maximum)[39] and Globalsolve (evaluation limit: maximum) in optimization package of the Maple® software.[40]

The Nafion 115 cell system. The system equipped with a Nafion 115 membrane has been used since the values for the diffusion coefficients of the four vanadium ionic species through this membrane are known from the literature.[22] Using this information, the remaining six parameters (contact resistance of the cell system, two reference rate constants at electrodes, the formal potential, the diffusion distance, and the potential gradient) can be estimated through the parameter estimation approach. Parameter estimation has been simultaneously carried out using four experimental voltage profiles of charging and discharging protocols for the first cycle (CC-CV charging and CC discharging for two different C-rates at C/20 and C/30). Also, for the best performance of the optimization problem, the diffusion distance and reference rate constants are expressed in term of an exponential function ($k_c = e^{-A}$, $k_a = e^{-B}$, and $\delta_{diff} = e^{-C}$), and indices (A,B, and C) of the exponential function are used as optimizing variables since the original parameters (diffusion distance and reference rate constants) are too small scale (~10^{-6}) to identify proper optimization values. In the main text, the original parameters are reported, but indices values of the exponential function are presented in open source codes.

- *Initial guesses.* The initial guesses for the diffusion distance, the potential gradients at C/30 and C/20, reference rate constants at positive and negative electrodes, the contact resistance, and the formal potential were 136.3889 um, 0.73×10^{-4} V/um, 0.105×10^{-3} V/um, 5.4037×10^{-7} m/s, 2.2116×10^{-6} m/s, 13.8104 Ω, 1.4362 V.

- *Lower and upper bounds.* The lower and upper bounds for the diffusion distance were 127 to 150.7331 um. The bounds for the potential gradients at C/30 and C/20 were given as 0.7×10^{-4} to 0.75×10^{-4} V/um and 0.1×10^{-3} and 0.11×10^{-3} V/um, respectively. The upper and lower bounds for reference rate constants at positive and negative electrodes were 5.0435×10^{-7} to 6.1601×10^{-7} m/s and 1.8506×10^{-6} to 2.2603×10^{-6} m/s, respectively. The upper and lower bounds for the contact resistance were 12 to 15 Ω. The bound for the formal potential was given as 1.43 to 1.45 V.

- ***Converged parameters.*** The converged parameters for the diffusion distance, the potential gradients at C/30 and C/20, reference rate constants at positive and negative electrodes, the contact resistance, and the formal potential are 147.8244 um, 0.749×10^{-4} V/um , 0.1×10^{-3} V/um , 0.5796×10^{-6} m/s, 2.2545×10^{-6} m/s, 14.4541 Ω, and 1.4451V, respectively. Also, the minimized MSE was 10.6269 mV.

The Nafion XL cell system. Voltage outputs from the model are fitted to experimental voltage data at C/30 during the first cycle. By doing this, diffusion coefficients of vanadium ions for other membranes, which have not yet been investigated, are estimated based on the predetermined other parameters in the Nafion 115 cell system. The Nafion XL membrane equipped static cell system has been considered, where diffusion coefficients have not been identified. While system parameters, including the contact resistance of the cell system, two reference rate constants at electrodes, and the formal potential remain the same as obtained in the Nafion 115 system, other six parameters including four diffusion coefficients of the ionic species through the Nafion XL membrane, the diffusion distance of the Nafion XL membrane, and the potential gradient inside the membrane are estimated through the parameter estimation approach. The diffusion distance and diffusion coefficients of four ionic species are expressed and scaled in term of exponential functions as well, where the indices appearing to the power of the number e are used as the parameters for optimization. In the main text, the original parameters are reported, but indices of exponential function are shown in open source codes.

- ***Initial guesses.*** The initial guesses for the diffusion distance, the potential gradient, and four diffusion coefficients of V^{2+}, V^{3+}, VO^{2+}, and VO_2^{+} were 100 um, 0.58×10^{-4} V/um, 9.1201×10^{-12} m^2/s , 3.9811×10^{-12} m^2/s, 2.4279×10^{-11} m^2/s , and 1.7378×10^{-11} m^2/s, respectively.

- ***Lower and upper bounds.*** The lower and upper bounds for the diffusion distance were 82.7241 to 102.0549 um. The bound for the potential gradient was given as 0.55×10^{-4} to 0.60×10^{-4} V/um. The upper and lower bounds for diffusion coefficients of V^{2+}, V^{3+}, VO^{2+}, and VO_2^{+} were 7.9329×10^{-12} to 9.3094×10^{-12} m^2/s and 3.0988×10^{-12} to 4.1830×10^{-12} m^2/s, 1.9906×10^{-11} to 3.1849×10^{-11} m^2/s, and 1.6963×10^{-11} to 1.7832×10^{-11} m^2/s, respectively.

- ***Converged parameters.*** The converged parameters for the diffusion distance, the potential gradient, and four diffusion coefficients of V^{2+}, V^{3+}, VO^{2+}, and VO_2^{+} are 101.9611 um, 0.559×10^{-4} V/um, 8.6987×10^{-12} m^2/s, 3.6324×10^{-12} m^2/s, 2.5969×10^{-11} m^2/s, and 1.7402×10^{-11} m^2/s, respectively. Also, the minimized error was 0.6927mV.

Results and Discussion

This section shows that redox battery performance can be studied and analyzed using the optimization-based robust modeling framework, including physics-based electrochemical models and parameter estimation techniques. Accordingly, the comparison of voltage profiles between model predictions and experimental data and the predicted vanadium ions concentration are presented in Figures 5, 6, and 7. A good agreement has been observed at low C-rates (~ C/10), having the low value of MSEs (see the parameter estimation section). This section also discusses how the proposed approach can contribute to the RFB model development, providing estimation results of a recently published zero-dimensional model which includes only uni-directional migration effects.[13] The importance and limitations of the proposed work and future work will be discussed as well.

The Nafion 115 cell system. The coulombic efficiency of the Nafion 115 system is 0.73 at C/30 and 0.81 at C/20 as shown in Figure 5. It shows that the higher current rates give the higher coulombic efficiency.[41] Figures 5a and 5b also illustrate the effects of migration and diffusion of the static cell system. To study and analyze the effects of those two main transport phenomena through the membrane, the simple model, which does not include diffusion and migration, is presented. There is no crossover of ions through the membrane in the simple model. In the simple model, therefore, Equations 5-8 and 13-16 in Table II and III are used for charging and discharging, respectively, with Equations 17-21 in Table IV and the parameters in Table VI and VII.

In Figure 5, the charging profile of the VRSB model, including diffusion and migration, is longer than that of the simple model, and the reverse is found for the discharging profile. Partial self-discharge of vanadium ions through the membrane is one of the main reasons for this capacity loss. To study this capacity loss in detail, Figure 6 describes the comparison of the predicted concentration of vanadium ions between the VRSB and simple model. Ideally, V^{2+} ions should only be generated from V^{3+} ions through an electrochemical reaction at the negative electrode during charging (see Figure 6b). In reality, V^{2+} ions are continuously depleted in negative electrolytes due to side reactions with VO^{2+}/VO_2^+ ions and crossover of V^{2+} ions through the membrane (see Figure 6a). Likewise, VO_2^+ ions should be only produced for charging (see Figure 6d), but they are also depleted in the positive electrolyte because of their crossover and side reactions giving rise to VO^{2+} ions (see Figure 6c). The self-discharge of

vanadium ions, which happens during charging, causes a slower charge until the cell is achieved at the maximum voltage. In contrast, this self-discharge leads to faster discharge and shorter discharge time. During discharge, V^{2+} and VO_2^+ ions are depleted due to electrochemical reactions at the negative electrode and their side reactions with other vanadium ions and crossover through the membrane, thereby dropping the concentration of V^{2+} and VO_2^+ ions faster (see Figure 6a and 6c). For this reason, the self-discharge of vanadium ions, which happens during discharge, causes a faster discharge until the cell achieves the minimum voltage. Importantly, the VRSBs/VRFBs do not produce any inert third compound, such as Li-ion SEI/plating, that can cause irreversible capacity loss.[42] Rather, side reactions in VRSBs/VRFBs are disproportionate reactions, which convert vanadium ions from one oxidation state to another state.[11]

***The Nafion XL cell system*.** Figure 7a presents the comparison of voltage profiles between model output and experimental data. Figures 7b and 7c show the predicted concentration of V^{2+}, V^{3+}, VO^{2+}, and VO_2^+ ions of the static cell system having Nafion XL membrane. Like the Nafion 115 system, the change in concentration of V^{2+}/V^{3+} ions is smaller than that of VO^{2+}/VO_2^+ ions during charging, and the reverse is found during discharging**.** The imbalance of vanadium ion concentration between the positive and negative electrolytes causes capacity loss/fade of VRSBs. The imbalance of the Nafion XL system is more severe than the system of Nafion 115.

Uni-directional migration. An approach to a zero-dimensional VRFB model, which includes uni-directional migration effects to the diffusion flux, was proposed recently.[13] However, the limitation of this model is that only VO^{2+} and VO_2^+ ions move from the positive to the negative electrolyte during charging, and only V^{2+} and V^{3+} ions move from the negative to the positive electrolyte during discharging, as shown in Figure S1 (see the uni-directional model section in the supplementary section).[13] For migration effects, in the model, the potential gradient inside the membrane ($=\nabla\phi$) was expressed as the potential drop from positive to negative sides divided by the diffusion distance ($=\frac{\phi_{neg}-\phi_{pos}}{\delta_{diff}}$). After that, the potential drop across the membrane was indirectly identified by using an equation ($\phi_{neg}-\phi_{pos}=\frac{I_{app}}{\sigma_{eff}}\frac{\delta_{diff}}{A_{cross}}$) consisting

of the effective conductivity ($=\sigma_{eff}$), the cell cross-sectional area($=A_{cross}$), applied current ($=I_{app}$), and the diffusion distance ($=\delta_{diff}$). In this formulation, however, it is not possible for migration effects to have the anti-directional flux to the diffusion flux since there are no ion sources from the opposite compartment.[13] In contrast, the proposed approach directly estimates the potential gradient inside a membrane thereby including both uni- and anti-directional migration effects having the more accurate prediction. Vanadium ions always face the potential gradient regardless of the order of models. This is an example showing how the proposed estimation approach can contribute to improving the model development, and why the parameter estimation techniques are essential for the accurate prediction of the battery performance. The same proposed approach to parameter estimation has been attempted using the uni-directional migration zero-dimensional model as shown in Figure S2. The minimized MSEs of the Nafion 115 system (C/30 and C/20) and the Nafion XL system (C/30) are 12.389 and 1.228 mV, respectively, which are larger MSEs than the full migration model of the proposed approach. Especially, the end part of the charge between model outputs and experimental data was not matched well. Detailed results of the parameter estimation are presented in the Parameter estimation section and Table S2 in the supplementary materials.

Importance of proposed work. The proposed parameter estimation technique can be used to track the effects of capacity loss/fade. As we mentioned earlier, one of the main reasons of the redox batteries' capacity loss/fade is ions' crossover through the membrane,[11] and this can be linked to transport and kinetic parameters. The proposed optimization-based approach can be used to update the transport and kinetic parameters or any degradation inputs of redox batteries within a short period. Any mismatch between model and data over cycles can be resolved with the updated parameters, and controls of the redox batteries with precise predictions based on the proposed work might lead to longer battery life and lower battery cost.

Limitations of proposed work. High-fidelity models for redox flow batteries are highly nonlinear and multidimensional systems, and use of these models will allow for more precise estimation of battery performance.[43] This study used a zero-dimensional physics-based electrochemical model, which describes vanadium ions' behavior of the redox battery system, but other chemical species, such as hydrogen, sulfate, and hydrogen sulfate, can also be included to achieve better prediction and accuracy of the model.[3, 13] Also, the proposed work

includes ion transport through only the membrane using bulk solutions at positive and negative electrolytes. Multi-dimensional models can include ion transport across entire cell (e.g., electrolytes, membranes, and electrodes). For this reason, experiments, simulations, and estimations have been conducted at low C-rates (~C/10), and the proposed zero-dimensional model of this paper has a good agreement up to C/10 rates (between experimental data and model outputs). For example, simulation results of other C-rates for two different systems (Nafion 115 system at C/10 and Nafion XL system at C/20) were presented in Figure S3. In this simulation, the potential gradient inside a membrane was estimated and for other parameters, the estimated values from the previous step were used. The proposed estimation approach in the next study will be implemented over full C-rates using more detailed models which include more ions and physics.

Open source codes and executable files

The main objective of this paper is to provide executable files and open source codes for models, experimental database, and estimation techniques so that the proposed approach can be pragmatically implemented from users' point of view. Most of the literature on parameter estimation of redox flow batteries only provides model equations, estimation methods, and simulation and estimation results.[18-20] In this case, however, if users want to estimate parameters of the redox battery system by following a way of estimation published in the literature, they need to install the specific computational software, write down model equations, and reproduce parameter estimation techniques. Although parameter estimation is a very active area of research in practical applications, this process is not an efficient way from a practical point of view. To resolve this issue, we provide open source codes and executable files written in Fortran (*see supplementary materials*). In the source codes, users can replace the model and experimental data in the original code with their own model and experimental data. The executable files can be used as an optimization tool for users to quickly address their parameter estimation problems for redox battery systems. For example, the executable file allows users to estimate parameters by simply inputting experimental conditions (e.g., applied current, voltage data, and time intervals) and bounds for the parameters. Users can execute the file without any special computational requirement including any software installation and a priori programming knowledge. This enables users to easily understand VRSB/VRFB models and parameter estimation approaches. Detailed instructions of the executable files is explained in

the Executable program section in the supplementary materials.

Target users. The executable file was designed for experimental researchers who are not familiar with mathematical approaches and or have the necessary computational infrastructure. Also, open source codes can be used by both modelers and experimental researchers to understand or modify redox flow cell models and optimization approaches.

Solver and optimization. The executable file was compiled with model equations, DAE solver with zero crossing (DASKR)[44], and the improved nondominated sorting genetic algorithm (NSGA-II).[45] NSGA-II has been one of the most widely used multi-objective optimization algorithm, which can identify and optimize the battery performance with fast speed and high accuracy.[45] In this paper, the algorithm was designed to include the single objective function by setting up the same multi-objective functions. In NSGA-II, the number of population size is 100, the max number of generation is 10, the crossover probability is 0.9, the mutation probability is 0.1, the iteration number is 5, the distribution index for crossover is 10, and the distribution index for mutation is 20.

Converged parameters. The same bounds used in the previous section were used for executable files. The difference of converged parameters optimized by NLPsolve/Globalsolve in Maple and NSGA-II with DASKR were found to be less than 10%. In the NSGA-II optimization, the converged parameters of the Nafion 115 system for the diffusion distance, the potential gradient at C/30 and C/20, reference rate constants at positive and negative electrodes, the contact resistance, and the formal potential are 133.9606 um, 0.7137 $\times 10^{-4}$ V/um, 0.1072×10^{-3} V/um, 5.8107×10^{-7} m/s, 2.1877×10^{-6} m/s , 12.6001 Ω, and 1.4321 V, respectively. Also, the converged parameters of the Nafion XL system for the diffusion distance, the potential gradient, and four diffusion coefficients of V^{2+}, V^{3+}, VO^{2+}, and VO_2^{+} are 93.861593529 um, 0.568456 V/um, 8.6707×10^{-12} m^2/s , 3.2975×10^{-12} m^2/s , 2.9156×10^{-11} m^2/s , 1.7049×10^{-11} m^2/s , respectively.

Conclusion

This work is an attempt to estimate all parameters of VRSBs using physics-based electrochemical engineering models. This study used a zero-dimensional electrochemical engineering model, which included mass balance equations of vanadium ions in addition to the other equations covering the aspects of cell voltage, formal and overpotential, the diffusion distance, and the potential gradient inside a membrane. This work illustrates that VRSB/VRFB

system can be studied and analyzed in detail based on the parameter estimation approaches, using physics-based electrochemical models. It also provides a way to study and analyze other RFBs based on parameter estimation techniques. Open source codes and executable files are provided, which enables users to quickly estimate parameters of the VRSB system. The proposed approach of parameter estimation is very generic and can be extended for estimation of parameters for other RFB models incorporating different chemistry as well as complexity (0-D to 3-D).

Acknowledgements.

This work was supported by the Clean Energy Institute located in University of Washington, Seattle and Washington Research Foundation. The battery modeling work has been supported by the Assistant Secretary for Energy Efficiency and Renewable Energy, Office of Vehicle Technologies of the U. S. Department of Energy through the Advanced Battery Material Research (BMR) Program (Battery500 Consortium). The battery experimental work has been supported by program manager Dr. Imre Gyuk through the U.S. Department of Energy, Office of Electricity Delivery and Energy Reliability. Sandia National Laboratories is a multi-mission laboratory managed and operated by National Technology and Engineering Solutions of Sandia, LLC., a wholly owned subsidiary of Honeywell International, Inc., for the U.S. Department of Energy's National Nuclear Security Administration under contract DE-NA0003525.

References

1. K. T. Cho, P. Ridgway, A. Z. Weber, S. Haussener, V. Battaglia, and V. Srinivasan, *Journal of The Electrochemical Society*, **159** (11), A1806-A1815 (2012).
2. *VanadiumCorp. "Integrity, Originality, Service." Redox Flow Batteries Charge Forward. Ios Services, Sept.-Oct. 2016. Web. 15 July 2017. Available: http://www.iosgeo.com/en/news/news-from-our-clients/redox-flow-batteries-charge-forward/*.
3. K. Knehr, E. Agar, C. Dennison, A. Kalidindi, and E. Kumbur, *Journal of The Electrochemical Society*, **159** (9), A1446-A1459 (2012).
4. D. You, H. Zhang, and J. Chen, *Electrochimica Acta*, **54** (27), 6827-6836 (2009).
5. K. Knehr and E. Kumbur, *Electrochemistry Communications*, **13** (4), 342-345 (2011).
6. H. Al-Fetlawi, A. Shah, and F. Walsh, *Electrochimica Acta*, **55** (1), 78-89 (2009).
7. G. Merei, S. Adler, D. Magnor, M. Leuthold, and D. U. Sauer, *Energy Procedia*, **46** 194-203 (2014).
8. H. Al-Fetlawi, A. Shah, and F. Walsh, *Electrochimica Acta*, **55** (9), 3192-3205 (2010).
9. A. Shah, R. Tangirala, R. Singh, R. Wills, and F. Walsh, *Journal of the Electrochemical society*, **158** (6), A671-A677 (2011).
10. A. Shah, M. Watt-Smith, and F. Walsh, *Electrochimica Acta*, **53** (27), 8087-8100 (2008).
11. A. Tang, J. Bao, and M. Skyllas-Kazacos, *Journal of Power Sources*, **196** (24), 10737-10747 (2011).
12. A. Shah, H. Al-Fetlawi, and F. Walsh, *Electrochimica Acta*, **55** (3), 1125-1139 (2010).
13. P. A. Boettcher, E. Agar, C. Dennison, and E. C. Kumbur, *Journal of The Electrochemical Society*, **163** (1), A5244-A5252 (2016).

14. Y. Lei, B. Zhang, B. Bai, and T. S. Zhao, *Journal of Power Sources*, **299** 202-211 (2015).
15. Y. A. Gandomi, T. A. Zawodzinski, and M. M. Mench, *ECS Transactions*, **61** (13), 23-32 (2014).
16. D. A. Beck, J. M. Carothers, V. R. Subramanian, and J. Pfaendtner, *AIChE J*, **62** (5), 1402-1416 (2016).
17. S. B. Lee, C. Pathak, V. Ramadesigan, W. Gao, and V. R. Subramanian, *Journal of The Electrochemical Society*, **164** (11), E3026-E3034 (2017).
18. Z. Wei, T. M. Lim, M. Skyllas-Kazacos, N. Wai, and K. J. Tseng, *Applied Energy*, **172** 169-179 (2016).
19. R. L. Fares, J. P. Meyers, and M. E. Webber, *Applied Energy*, **113** 189-198 (2014).
20. Z. Wei, K. J. Tseng, N. Wai, T. M. Lim, and M. Skyllas-Kazacos, *Journal of Power Sources*, **332** 389-398 (2016).
21. E. Wiedemann, A. Heintz, and R. Lichtenthaler, *Journal of membrane science*, **141** (2), 215-221 (1998).
22. C. Sun, J. Chen, H. Zhang, X. Han, and Q. Luo, *Journal of Power Sources*, **195** (3), 890-897 (2010).
23. J. Li, L. Wang, C. Lyu, H. Wang, and X. Liu, *Journal of Power Sources*, **307** 220-230 (2016).
24. M. Skyllas-Kazacos and L. Goh, *Journal of membrane science*, **399** 43-48 (2012).
25. D. Aaron, C.-N. Sun, M. Bright, A. B. Papandrew, M. M. Mench, and T. A. Zawodzinski, *ECS Electrochemistry Letters*, **2** (3), A29-A31 (2013).
26. M. Miller, A. Bourke, N. Quill, J. Wainright, R. Lynch, D. Buckley, and R. Savinell, *Journal of The Electrochemical Society*, **163** (9), A2095-A2102 (2016).
27. H. D. Pratt, N. S. Hudak, X. Fang, and T. M. Anderson, *Journal of Power Sources*, **236** 259-264 (2013).
28. *Sigma-Aldrich. Web. 15 July 2017.* *Available: http://www.sigmaaldrich.com/catalog/product/aldrich/233706?lang=en®ion=US*.
29. *Sigma-Aldrich. Web. 16 July 2017.* *Available: http://www.sigmaaldrich.com/catalog/product/aldrich/339741?lang=en®ion=US*.
30. S. Shi, A. Z. Weber, and A. Kusoglu, *Journal of Membrane Science*, **516** 123-134 (2016).
31. S. Motupally, A. J. Becker, and J. W. Weidner, *Journal of The Electrochemical Society*, **147** (9), 3171-3177 (2000).
32. *Graphite. Web. 15 July 2017. Available: http://poco.com/MaterialsandServices/Graphite.aspx*.
33. *AMETEK SI. Web. 15 July 2017. Available: http://www.ameteksi.com/products/potentiostats/single-channel/12xx-series*.
34. *Adams & Chittenden Scientific Glass Home. Web. 16 July 2017.* *Available: http://www.adamschittenden.com/index.php*.
35. *Tenney Environmental Walk In Room." Manufacturer of Industrial Ovens and Test Chambers. Web. 16 July 2017. Available: https://www.thermalproductsolutions.com/product/tenney-environmental-walk-in-room*.
36. O. Levenspiel, *Industrial & engineering chemistry research*, **38** (11), 4140-4143 (1999).
37. T. E. Springer, T. Zawodzinski, and S. Gottesfeld, *Journal of the Electrochemical Society*, **138** (8), 2334-2342 (1991).
38. V. Ramadesigan, K. Chen, N. A. Burns, V. Boovaragavan, R. D. Braatz, and V. R. Subramanian, *Journal of The Electrochemical Society*, **158** (9), A1048-A1054 (2011).
39. *Maplesoft. Web. 24 January 2018.* *Available:* *https://www.maplesoft.com/support/help/maple/view.aspx?path=Optimization%2fGeneral%2fOptions*.
40. J. D. Pintér, D. Linder, and P. Chin, *Optimisation Methods and Software*, **21** (4), 565-582 (2006).
41. A. Z. Weber, M. M. Mench, J. P. Meyers, P. N. Ross, J. T. Gostick, and Q. Liu, *Journal of Applied Electrochemistry*, **41** (10), 1137-1164 (2011).
42. P. Verma, P. Maire, and P. Novák, *Electrochimica Acta*, **55** (22), 6332-6341 (2010).
43. M. T. Lawder, B. Suthar, P. W. Northrop, S. De, C. M. Hoff, O. Leitermann, M. L. Crow, S. Santhanagopalan, and V. R. Subramanian, *Proceedings of the IEEE*, **102** (6), 1014-1030 (2014).
44. L. R. Petzold, *Computer Methods in Applied Mechanics and Engineering*, **75** (1-3), 77-89 (1989).
45. K. Deb, A. Pratap, S. Agarwal, and T. Meyarivan, *IEEE transactions on evolutionary computation*, **6** (2), 182-197 (2002).
46. A. Tang, J. Bao, and M. Skyllas-Kazacos, *Journal of Power Sources*, **216** 489-501 (2012).

Figure captions

Figure 1: Schematic of the laboratory-scale VRSB system. (a) An actual image of the system. (b) Specification of the system.

Figure 2: Crossover of vanadium ions through the membrane by diffusion and migration during (a) charging and (b) discharging.

Figure 3: Side reactions caused by crossover of vanadium ions through the membrane durging charging.

Figure 4. Parameter estimation of the static cell system with charging/ discharging curves at different C-rates.

Figure 5: Comparison of voltage profiles between battery model outputs and experimental data from the static cell system including Nafion 115, and analysis of effects of diffusion and migration, using the simple model.

Figure 6: Comparison of predicted concentration of the different vanadium ions between the VRSB model and simple model at C/30.

Figure 7: Comparison of voltage profiles between battery model outputs and experimental data, and predicted vanadium ion concentrations vs. capacity, for the static cell system including Nafion XL membrane at the first cycle.

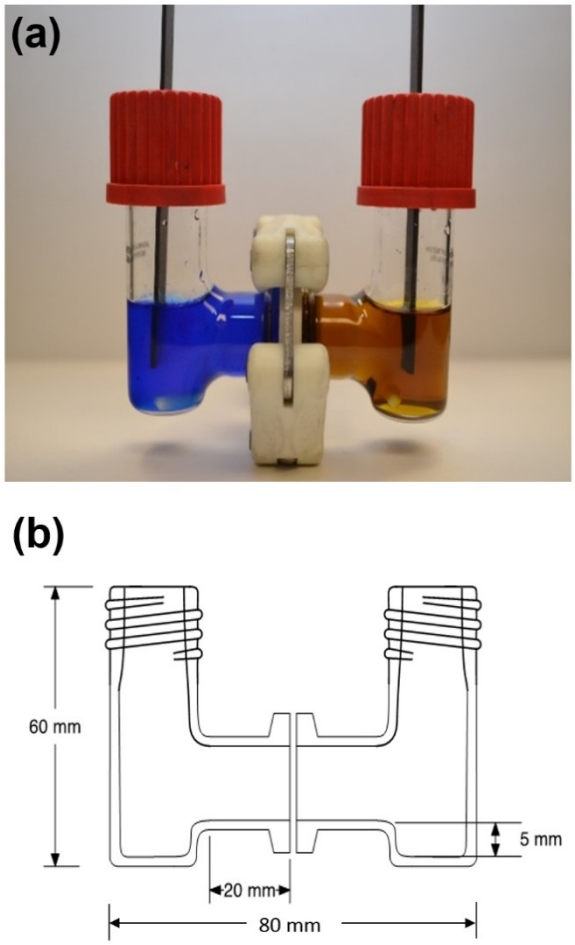

Figure 1. Schematic of the laboratory-scale VRSB system. (a) An actual image of the system. (b) Specification of the system. The static cell system has advantages of being easy and simple to implement and a quick understanding of the performance of the RFBs. Coupling with electrochemical engineering models for VRSBs helps modelers estimate parameters and analyze cell performance efficiently.

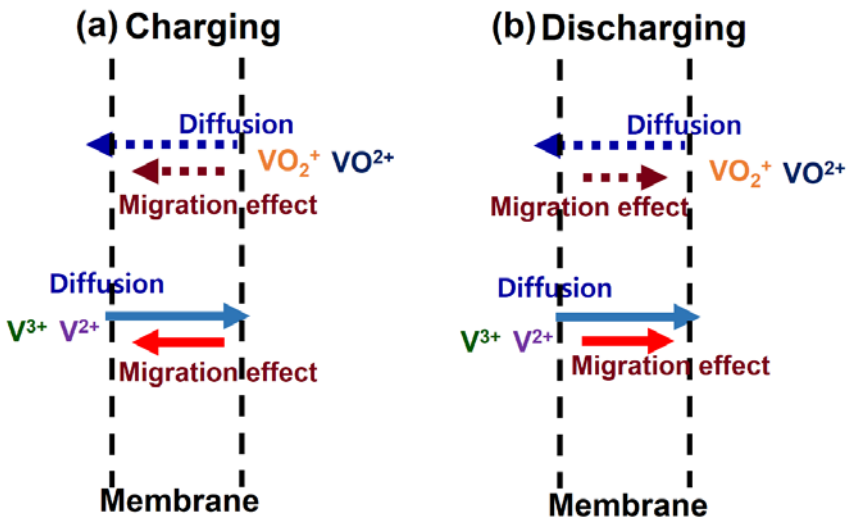

Figure 2. Crossover of vanadium ions through the membrane by diffusion and migration during (a) charging and (b) discharging. A blue colored dotted arrow indicates VO^{2+}/VO_2^+ diffusion (see the first arrow from the top in (a) Charge and (b) Discharge), a wine colored dotted arrow represents VO^{2+}/VO_2^+ migration (see the second arrow from the top in (a) Charging and (b) Discharging), a sky-blue colored solid arrow shows V^{2+} / V^{3+} diffusion (see the third arrow from the top in (a) Charging and (b) Discharging), and a red colored solid arrow represents V^{2+}/V^{3+} migration (see the fourth arrow from the top in (a) Charging and (b) Discharging)**.** The main transport phenomena of the static system are diffusion and migration. The diffusion of vanadium ions through the membrane has the same direction regardless of charging and discharging and the direction of migration through the membrane is affected by charging / discharging conditions.

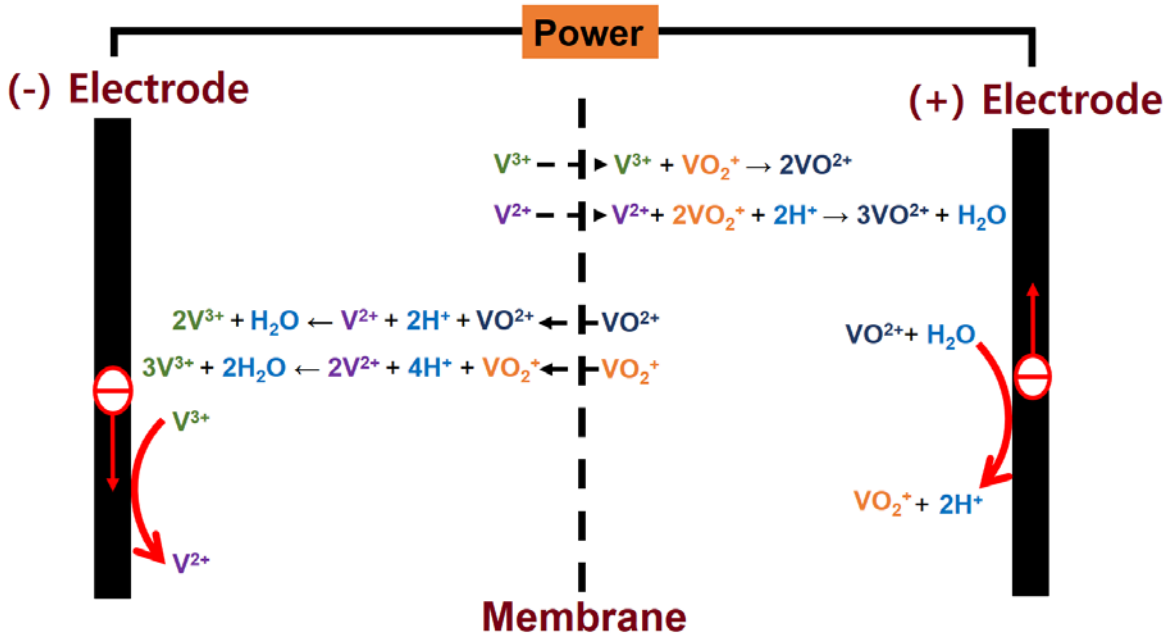

Figure 3. Side reactions caused by crossover of vanadium ions through the membrane durging charging. One mole of V^{2+}, which moves across the membrane from the negative electrolyte, reacts with two moles of VO_2^+ in the positive electrolytes producing three moles of VO^{2+}. One mole of V^{3+} crossover from the negative electrolyte causes a chemical reaction with one mole of VO_2^+ producing two moles of VO^{2+} in the positive electrolyte. Similarly, in the negative electrolyte, two moles of V^{3+} are produced by a chemical reaction between one mole of V^{2+} and one mole of VO^{2+}, which moves from the positive electrolyte, and three moles of V^{3+} are produced by a chemical reaction between two moles of V^{2+} and one mole of VO_2^+, which moves from the positive electrolyte.

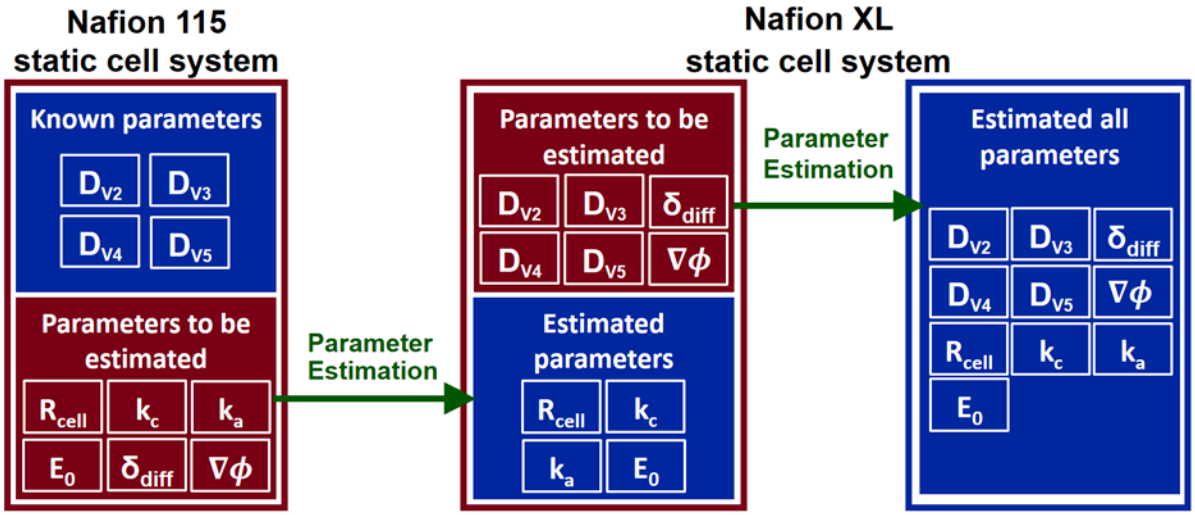

Figure 4. Parameter estimation of the static cell system with charging/ discharging curves at different C-rates. We show a way of estimating all parameters in a model, which can help analyze and study the performance of the cell system.

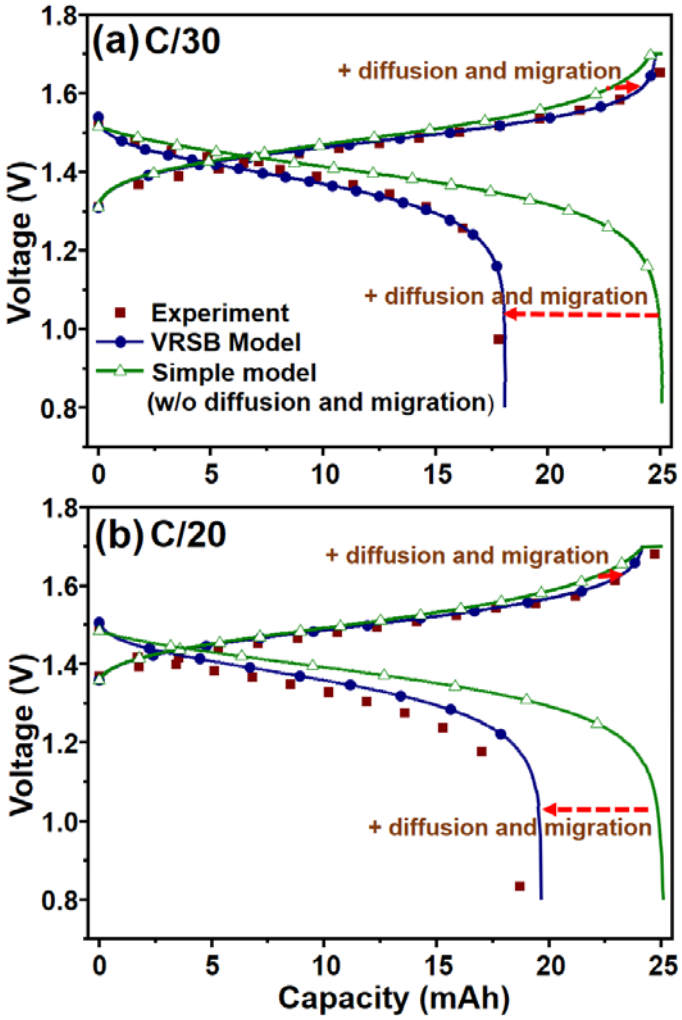

Figure 5. Comparison of voltage profiles between battery model outputs and experimental data from the static cell system including Nafion 115, and analysis of effects of diffusion and migration, using the simple model. Voltage profiles at (a) C/30 and (b) C/20 (Experimental data: wine color and filled square dots, the VRSB model: blue color and filled circle plot, and the simple model: green color and empty triangle plot). Parameters were simultaneously estimated at C/20 and C/30, minimizing the mean of the sum-of-squared differences between the model and experiment outputs.

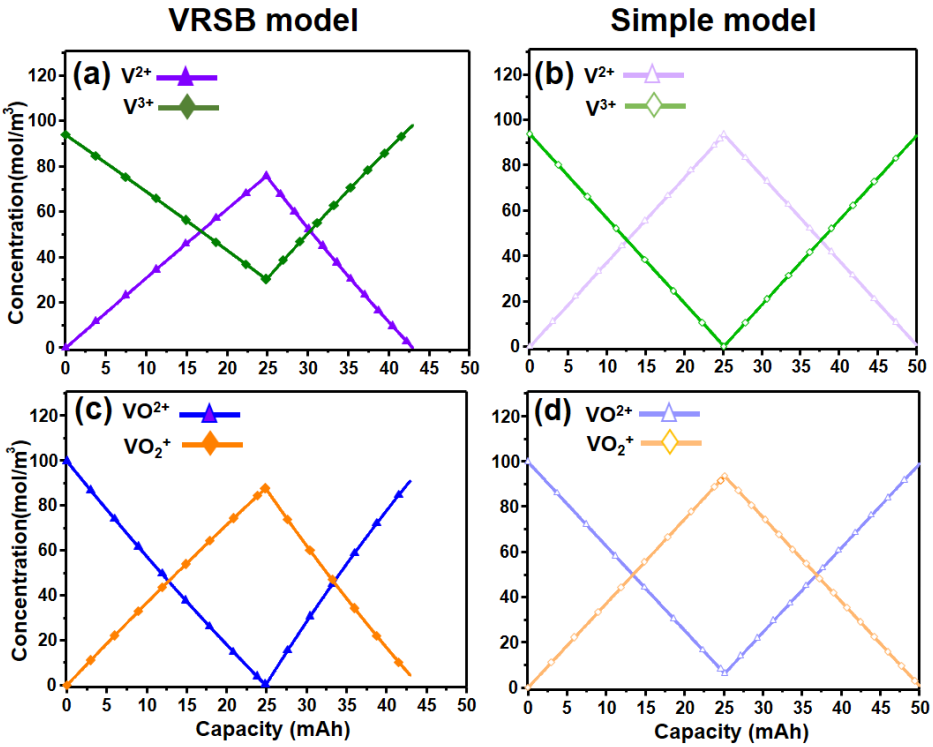

Figure 6. Comparison of predicted concentration of the different vanadium ions between the VRSB model and simple model at C/30. (a) V^{2+} (purple color and filled triangle) and V^{3+} (green color and filled diamon) concentration profiles from the VRSB model at C/30, (b) V^{2+} (light purple color and empty triangle) and V^{3+} (light green color and empty diamon) concentration profiles from the simple model at C/30, (c) VO^{2+} (blue color and filled triangle) and VO_2^+ (orange color and filled diamond) concentration profiles from the VRSB model at C/30, and (d) VO^{2+} (light blue color and empty triangle) and VO_2^+ (light orange color and empty diamond) concentration profiles from the simple model at C/30. An imbalance of the vanadium ion concentration between the positive and negative electrolytes causes capacity loss/fade of VRSB/VRFBs.

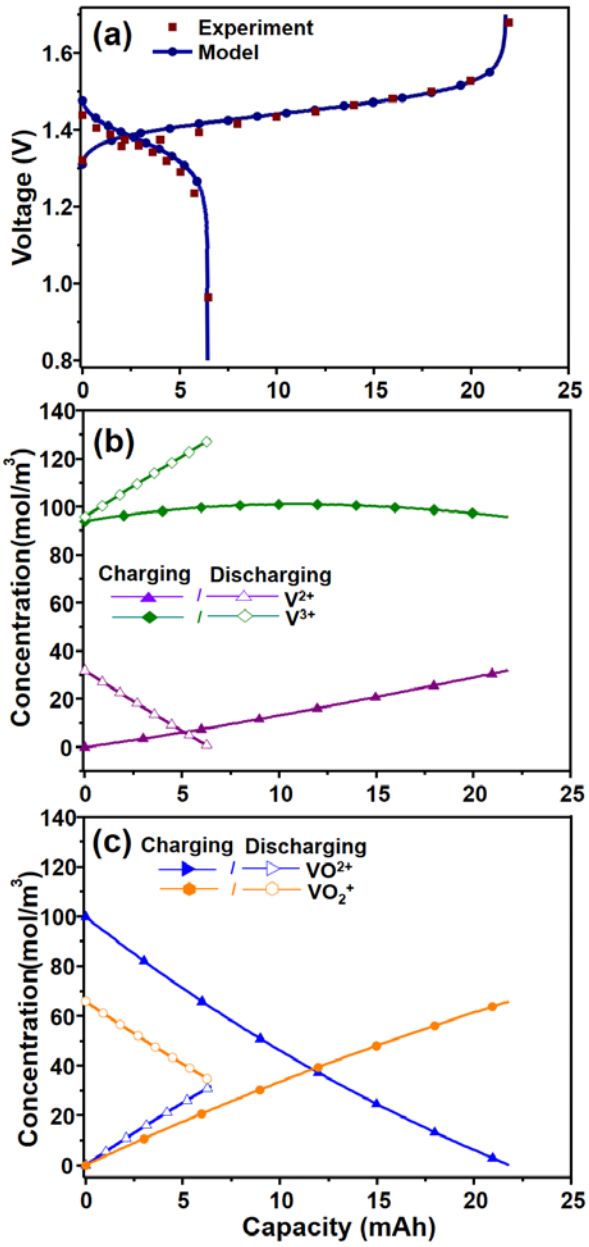

Figure 7. Comparison of voltage profiles between battery model outputs and experimental data, and predicted vanadium ion concentrations vs. capacity, for the static cell system including Nafion XL membrane at the first cycle. (a) Voltage profiles from experiment data (wine color and filled square) and model outputs (blue color and filled circle) at C/30 (b) V^{2+} (charge: green color and filled diamond, and discharge: green color and empty diamond) and V^{3+} (charge: purple color and filled triangle, and discharge: purple color and empty triangle) concentration profiles at C/30. (c) VO^{2+} (charge: blue color and filled triangle, and discharge: blue color and empty triangle) and VO_2^+ (charge: orange color and filled diamond, and discharge: orange color and empty diamond) concentration profiles at C/30. Parameters were estimated at C/30 based on cell system parameters predetermined in the Nafion 115 system, minimizing the mean of sum-of-squared differences between the model and experiment outputs.

Table Captions

Table I: Selected Physics-based Electrochemical Models of Vanadium Redox Flow Batteries

Table II: Governing Equations for Charging Process of All-Vanadium Redox Static Cells

Table III. Governing Equations for Discharging Process of All-Vanadium Redox Static Cells

Table IV. Additional Equations for All-Vanadium Redox Static Batteries

Table V. Variables for All-Vanadium Redox Static Batteries

Table VI. Parameters of All-Vanadium Redox Static Batteries

Table VII. Estimated Parameters of All-Vanadium Redox Static Batteries

Table I. Selected Physics-based Electrochemical Engineering Models of Vanadium Redox Flow Batteries

Model	Ions and molecules included in models									Ions and molecules transport across electrodes			through the membrane			Gassing side reactions		Thermal effects	Transport theory	Key points	Ref. (Year)
	V^{2+}	V^{3+}	VO^{2+}	VO_2^+	H^+	OH^-	HSO_4^-	SO_4^{2-}	H_2O	Diff.	Mig.	Conv.	Diff.	Mig.	Conv.	H_2	O_2				
Zero-dimensional models																					
Shah *et. al.*	O	O	O	O	O	X	X	X	O	N/A · Zero-dimensional models assume that bulk electrolyte transport happens across the membrane from positive and negative electrodes.			X H^+: No constraints H_2O: Osmotic drag	X	X	X	X	Isothermal	Not Applicable	Allowed only H^+ and H_2O crossover through the membrane	9 (2011)
Tang *et. al.*	O	O	O	O	X	X	X	X	X				O V^{2+}, V^{3+}, VO^{2+}, and VO_2^+	X	X	Used current efficiency factor		Isothermal	Dilute solution	Demonstrated the static cell model	11 (2011)
Tang *et. al*	O	O	O	O	X	X	X	X	X	· There is concentration gradient across electrodes in real system, but zero-dimensional models are important for control and prediction for long cycles			O V^{2+}, V^{3+}, VO^{2+}, and VO_2^+	X	X	X	X	Thermal	Dilute solution	Coupled thermal effects with mass balance equations	46 (2012)
Boettcher *et. al.*	O	O	O	O	O	X	O	O	O				O All ions except for OH^-, and SO_4^{2-}	O	O	X	X	Isothermal	Dilute solution	Limitation is uni-directional flux for migration.	13 (2016)
One-dimensional models (assuming bulk electrolytes at positive and negative)																					
Gandomi *et. al.*	X	X	X	X	O	X	O	X	O	N/A · One-dimensional membrane models assume positive and negative have bulk electrolyte transport.			N/A (concentrated solution) H^+, HSO_4^-, and H_2O			X	X	Isothermal	Concentrated solution	Assumed that only H^+, HSO_4^-, and H_2O can cross the membrane	14 (2014)
Lei *et. al.*	O	O	O	O	O	X	O	X	X				O All ions except for SO_4^{2-}, OH^- and H_2O	O	O	X	X	Isothermal	Dilute solution	Included Donnan effects	15 (2015)
Two-dimensional models																					
Shah *et. al.*	O	O	O	O	O	X	O	O	O	O (V^{2+}, V^{3+}, VO^{2+}, and VO_2^+)	O	O	O (H^+, HSO_4^-, and H_2O)	O	O	O	X	Isothermal	Dilute solution	No vanadium ions crossover through the membrane and side reactions of the same	12 (2010)
Al-Fetlawi *et. al.*	O	O	O	O	O	X	O	O	O	O (V^{2+}, V^{3+}, VO^{2+}, and VO_2^+	O	O	X (H^+, HSO_4^-, and H_2O)	X	X	X	X	Thermal	Dilute solution		8 (2009)
Knehr *et. al.*	O	O	O	O	O	X	O	O	O	O All ions except for SO_4^{2-}, and OH^-	O	O	O	O	O	X	X	Isothermal	Dilute solution	Implemented improved OCV and Donnan potential	3 (2012)

*Diffusion (Diff.). Migration (Mig.). Convection (Conv.). Not Applicable (N/A).

Table II. Governing Equations of All-Vanadium Redox Static Batteries (Charging Process)

Accumula	**=**	**+ In – Out** (Diffusion terms)	(Migration terms)	**No.**
VRSB Model (Diffusion + Migration)				
$V_r \frac{dC_{V^{2+}}(t)}{dt}$	$= +\frac{j_{app}}{F} A_{elec}$	$-\left(D_{V^{2+}} C_{V^{2+}}(t) + 2D_{VO_2^+} C_{VO_2^+}(t) + D_{VO^{2+}} C_{VO^{2+}}(t)\right)\frac{A_{mem}}{\delta_{diff}}$	$-2\left(D_{VO^{2+}} C_{VO^{2+}}(t) + D_{VO_2^+} C_{VO_2^+}(t) - D_{V^{2+}} C_{V^{2+}}(t)\right)\frac{F}{RT} A_{mem} \nabla\phi$	**[1]**
$V_r \frac{dC_{V^{3+}}(t)}{dt}$	$= -\frac{j_{app}}{F} A_{elec}$	$-\left(D_{V^{3+}} C_{V^{3+}}(t) - 3D_{VO_2^+} C_{VO_2^+}(t) - 2D_{VO^{2+}} C_{VO^{2+}}(t)\right)\frac{A_{mem}}{\delta_{diff}}$	$+\left(4D_{VO^{2+}} C_{VO^{2+}}(t) + 3D_{VO_2^+} C_{VO_2^+}(t) + 3D_{V^{3+}} C_{V^{3+}}(t)\right)\frac{F}{RT} A_{mem} \nabla\phi$	**[2]**
$V_r \frac{dC_{VO^{2+}}(t)}{dt}$	$= -\frac{j_{app}}{F} A_{elec}$	$-\left(D_{VO^{2+}} C_{VO^{2+}}(t) - 3D_{V^{2+}} C_{V^{2+}}(t) - 2D_{V^{3+}} C_{V^{3+}}(t)\right)\frac{A_{mem}}{\delta_{diff}}$	$-2\left(D_{VO^{2+}} C_{VO^{2+}}(t) + 3D_{V^{2+}} C_{V^{2+}}(t) + 3D_{V^{3+}} C_{V^{3+}}(t)\right)\frac{F}{RT} A_{mem} \nabla\phi$	**[3]**
$V_r \frac{dC_{VO_2^+}(t)}{dt}$	$= +\frac{j_{app}}{F} A_{elec}$	$-\left(D_{VO_2^+} C_{VO_2^+}(t) + 2D_{V^{2+}} C_{V^{2+}}(t) + D_{V^{3+}} C_{V^{3+}}(t)\right)\frac{A_{mem}}{\delta_{diff}}$	$-\left(D_{VO_2^+} C_{VO_2^+}(t) - 4D_{V^{2+}} C_{V^{2+}}(t) - 3D_{V^{3+}} C_{V^{3+}}(t)\right)\frac{F}{RT} A_{mem} \nabla\phi$	**[4]**
Simple model (w/o diffusion and migration)				
$V_r \frac{dC_{V^{2+}}(t)}{dt}$	$= +\frac{j_{app}}{F} A_{elec}$			**[5]**
$V_r \frac{dC_{V^{3+}}(t)}{dt}$	$= -\frac{j_{app}}{F} A_{elec}$			**[6]**
$V_r \frac{dC_{VO^{2+}}(t)}{dt}$	$= -\frac{j_{app}}{F} A_{elec}$			**[7]**
$V_r \frac{dC_{VO_2^+}(t)}{dt}$	$= +\frac{j_{app}}{F} A_{elec}$			**[8]**

Table III. Governing Equations of All-Vanadium Redox Static Batteries (Discharging Process)

Accum. =	**+In – Out + gen. / loss** (Diffusion terms)	(Migration terms)	**No.**

VRSB Model (Diffusion + Migration)

$$V_r \frac{dC_{V^{2+}}(t)}{dt} = -\frac{j_{app}}{F} A_{elec} \quad -\left(D_{V^{2+}} C_{V^{2+}}(t) + 2D_{VO_2^+} C_{VO_2^+}(t) + D_{VO^{2+}} C_{VO^{2+}}(t)\right)\frac{A_{mem}}{\delta_{diff}} \quad -2\left(D_{V^{2+}} C_{V^{2+}}(t) - D_{VO^{2+}} C_{VO^{2+}}(t) - D_{VO_2^+} C_{VO_2^+}(t)\right)\frac{F}{RT} A_{mem} \nabla\phi \quad \textbf{[9]}$$

$$V_r \frac{dC_{V^{3+}}(t)}{dt} = +\frac{j_{app}}{F} A_{elec} \quad -\left(D_{V^{3+}} C_{V^{3+}}(t) - 3D_{VO_2^+} C_{VO_2^+}(t) - 2D_{VO^{2+}} C_{VO^{2+}}(t)\right)\frac{A_{mem}}{\delta_{diff}} \quad -\left(3D_{V^{3+}} C_{V^{3+}}(t) + 4D_{VO^{2+}} C_{VO^{2+}}(t) + 3D_{VO_2^+} C_{VO_2^+}(t)\right)\frac{F}{RT} A_{mem} \nabla\phi \quad \textbf{[10]}$$

$$V_r \frac{dC_{VO^{2+}}(t)}{dt} = +\frac{j_{app}}{F} A_{elec} \quad -\left(D_{VO^{2+}} C_{VO^{2+}}(t) - 3D_{V^{2+}} C_{V^{2+}}(t) - 2D_{V^{3+}} C_{V^{3+}}(t)\right)\frac{A_{mem}}{\delta_{diff}} \quad +2\left(3D_{V^{2+}} C_{V^{2+}}(t) + 3D_{V^{3+}} C_{V^{3+}}(t) + D_{VO^{2+}} C_{VO^{2+}}(t)\right)\frac{F}{RT} A_{mem} \nabla\phi \quad \textbf{[11]}$$

$$V_r \frac{dC_{VO_2^+}(t)}{dt} = -\frac{j_{app}}{F} A_{elec} \quad -\left(D_{VO_2^+} C_{VO_2^+}(t) + 2D_{V^{2+}} C_{V^{2+}}(t) + D_{V^{3+}} C_{V^{3+}}(t)\right)\frac{A_{mem}}{\delta_{diff}} \quad -\left(4D_{V^{2+}} C_{V^{2+}}(t) + 3D_{V^{3+}} C_{V^{3+}}(t) - D_{VO_2^+} C_{VO_2^+}(t)\right)\frac{F}{RT} A_{mem} \nabla\phi \quad \textbf{[12]}$$

Simple model (w/o diffusion and migration)

$$V_r \frac{dC_{V^{2+}}(t)}{dt} = -\frac{j_{app}}{F} A_{elec} \quad \textbf{[13]}$$

$$V_r \frac{dC_{V^{3+}}(t)}{dt} = +\frac{j_{app}}{F} A_{elec} \quad \textbf{[14]}$$

$$V_r \frac{dC_{VO^{2+}}(t)}{dt} = +\frac{j_{app}}{F} A_{elec} \quad \textbf{[15]}$$

$$V_r \frac{dC_{VO_2^+}(t)}{dt} = -\frac{j_{app}}{F} A_{elec} \quad \textbf{[16]}$$

Table IV. Additional Equations of All-Vanadium Redox Static Batteries

	No.
$E_{cell}(t) = E_{cell}^{rev}(t) - j_{app}A_{electrode}R_{contact} - j_{app}\frac{d}{\sigma_{mem}} + \eta_2(t) - \eta_1(t)$	[17]
$E_{cell}^{rev}(t) = E_0 + \frac{RT}{F}\ln\left(\frac{C_{V^{2+}}(t)C_{VO_2^+}(t)}{C_{V^{3+}}(t)C_{VO^{2+}}(t)}\right)$	[18]
$\eta_1(t) = -\frac{2RT}{F}\arcsin\left(\frac{i_{app}}{2Fk_a\sqrt{C_{V^{3+}}(t)C_{V^{2+}}(t)}}\right),\ \eta_2(t) = \frac{2RT}{F}\arcsin\left(\frac{i_{app}}{2Fk_c\sqrt{C_{VO^{2+}}(t)C_{VO_2^+}(t)}}\right)$	[19]
$k_a = k_{a,ref}\exp\left(-\frac{F}{E_0^a}\frac{1}{R}(\frac{1}{T_{ref}} - \frac{1}{T})\right),\ k_c = k_{c,ref}\exp\left(-\frac{F}{E_0^c}\frac{1}{R}(\frac{1}{T_{ref}} - \frac{1}{T})\right)$	[20]
$\sigma_{mem} = (0.5139\lambda - 0.326)\exp\left(1268(\frac{1}{303} - \frac{1}{T})\right)$	[21]

Table V. Variables of All-Vanadium Redox Static Batteries

Symbol	Variable	Units
$C_{V^{2+}}(t)$	Concentration of Vanadium (II)	$\mathrm{mol\,m^{-3}}$
$C_{V^{3+}}(t)$	Concentration of Vanadium (III)	$\mathrm{mol\,m^{-3}}$
$C_{VO^{2+}}(t)$	Concentration of Vanadium (IV)	$\mathrm{mol\,m^{-3}}$
$C_{VO_2^+}(t)$	Concentration of Vanadium (V)	$\mathrm{mol\,m^{-3}}$
$E_{cell}(t)$	Cell voltage	V
$E_{cell}^{rev}(t)$	Open circuit voltage	V
$\eta_1(t)$	Overpotential at anode	V
$\eta_2(t)$	Overpotential at cathode	V

Table VI. Parameters of All-Vanadium Redox Static Batteries			
Symbol	**Parameter**	**Values**	**Units**
d	Thickness of membrane - Nafion 115	127×10^{-6}	m
	- Nafion XL	27.5×10^{-6}	
A_{mem}	Cross sectional area of the membrane	1.76625×10^{-4}	m^2
A_{elec}	Surface area of the electrode for reaction	2.3×10^{-4}	m^2
V_r	Volume of electrolyte	10^{-5}	m^3
T	Temperature	298	K
i_{app}	Current density	$C/20: 1.34\times10^{-3}$	$A\,m^{-2}$
		$C/30: 0.89\times10^{-3}$	
F	Faraday constant	96485.3365	$s\,A\,mol^{-1}$
λ	The membrane water content	22	
R	Ideal gas constant	8.314	$J\,K^{-1}\,mol^{-1}$
$D_{V^{2+}}$	V^{2+} diffusion coefficient of Nafion 115	0.87683×10^{-11}	$m^2\,s^{-1}$
$D_{V^{3+}}$	V^{3+} diffusion coefficient of Nafion 115	0.32217×10^{-11}	$m^2\,s^{-1}$
$D_{VO^{2+}}$	VO^{2+} diffusion coefficient of Nafion 115	0.6825×10^{-11}	$m^2\,s^{-1}$
$D_{VO_2^+}$	VO_2^+ diffusion coefficient of Nafion 115	0.5897×10^{-11}	$m^2\,s^{-1}$
E_0^a	Reference potential at anode reaction	-0.26	V
E_0^c	Reference potential at cathode reaction	1.004	V

Table VII. Estimated Parameters of All-Vanadium Redox Static Batteries

Symbol	Parameter	Lower bound	Upper bound	Initial guess	Final value (Units)
$R_{contact}$	Resistance	12	15	13.8104	14.4541 (Ω)
$k_{c,ref}$	Reference rate constant at positive electrode	5.0435×10^{-7}	6.1601×10^{-7}	5.4037×10^{-7}	0.5796×10^{-6} ($m\,s^{-1}$)
$k_{a,ref}$	Reference rate constant at negative electrode	1.8506×10^{-6}	2.2603×10^{-6}	2.2116×10^{-6}	2.2545×10^{-6} ($m\,s^{-1}$)
E_0	Formal potential	1.43	1.45	1.4362	1.4451 (V)
δ_{diff}	Diffusion distance				
	Nafion 115	127	150.7331	136.3889	147.8244 (um)
	Nafion XL	82.7241	102.0549	100	101.9611 (um)
$\nabla\phi$	Potential gradient				
	Nafion 115 at C/30	0.7×10^{-4}	0.75×10^{-4}	0.73×10^{-4}	0.749×10^{-4} (V / um)
	At C/20	0.1×10^{-3}	0.11×10^{-3}	0.105×10^{-3}	0.1×10^{-3} (V / um)
	Nafion XL system	0.55×10^{-4}	0.6×10^{-4}	0.58×10^{-4}	0.559×10^{-4} (V / um)
$D_{V^{2+}}$	V^{2+} diffusion coefficient for Nafion XL	7.9329×10^{-12}	9.3094×10^{-12}	9.1201×10^{-12}	8.6987×10^{-12} ($m^2\,s^{-1}$)
$D_{V^{3+}}$	V^{3+} diffusion coefficient for Nafion XL	3.0988×10^{-12}	4.1830×10^{-12}	3.9811×10^{-12}	3.6324×10^{-12} ($m^2\,s^{-1}$)
$D_{VO^{2+}}$	VO^{2+} diffusion coefficient for Nafion XL	1.9906×10^{-11}	3.1849×10^{-11}	2.4279×10^{-11}	2.5969×10^{-11} ($m^2\,s^{-1}$)
$D_{VO_2^+}$	VO_2^+ diffusion coefficient for Nafion XL	1.6963×10^{-11}	1.7832×10^{-11}	1.7378×10^{-11}	1.7402×10^{-11} ($m^2\,s^{-1}$)

Supplementary Materials

Estimation of Transport and Kinetic Parameters of Vanadium Redox Batteries Using Static Cells and Electrochemical Models

Seong Beom Lee,[a,1] Harry D. Pratt III,[b,1] Travis M. Anderson,[b,1] Venkatasailanathan Ramadesigan,[c, 2] Kishalay Mitra,[d] Babu R. Chalamala,[b,2], and Venkat R. Subramanian [a, e, 2,3]

[a] Department of Chemical Engineering, University of Washington, Seattle, WA 98195, USA
[b] Sandia National Laboratories, Albuquerque, NM 87185, USA
[c] Department of Energy Science and Engineering, Indian Institute of Technology Bombay, Powai, Mumbai, Maharashtra 400076, India
[d] Department of Chemical Engineering, Indian Institute of Technology Hyderabad, Kandi, Sangareddy, Telangana 502285, INDIA
[e] Pacific Northwest National Laboratory, Richland, WA 99354, USA

[1] Electrochemical Society Student Member
[2] Electrochemical Society Active Member
[3] Corresponding Author, Tel: +1-206-543-2271; Fax: +1-206-543-3778
Email: vsubram@uw.edu

SM 1. Uni-directional migration model. All relevant equations (Equations 1S-8S and 17-24 in Table SI and IV, respectively), variables (Table V), and parameters (Table VI), which are used to model and simulate the zero-dimensional model that describes uni-directional migration, are listed in Tables SI and IV-VI.

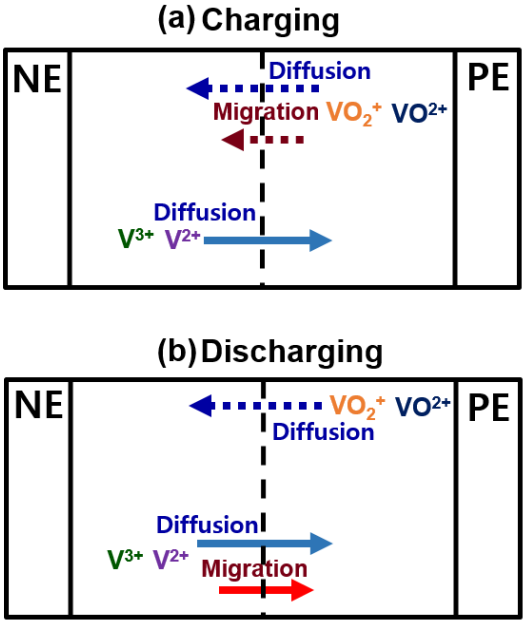

Figure S1. Crossover of vanadium ions through the membrane in the uni-directional migration model during (a) charging and (b) discharging. PE and NE represent positive and negative electrodes, respectively. A blue colored dotted arrow indicates VO^{2+}/VO_2^+ diffusion (see the first arrow from the top in (a) Charge and (b) Discharge), a wine colored dotted arrow represents VO^{2+}/VO_2^+ migration (see the second arrow from the top in (a) Charging), a sky-blue colored solid arrow shows V^{2+} / V^{3+} diffusion (see the third arrow from the top in (a) Charging and the second arrow from the top in (b) Discharging), and a red colored solid arrow represents V^{2+}/V^{3+} migration (see the third arrow from the top in (b) Discharging)**.**

SM 2. Parameter estimation. The comparison of voltage profiles between model outputs and experimental data is presented as shown in Figure S2 (Nafion 115 and Nafion XL system). The initial guesses, bounds, converged parameters, and minimized MSE are summarized in Table S2, and the values in Table S2 were rounded off to the fifth decimal place (original values are presented in the text in the supplementary materials).

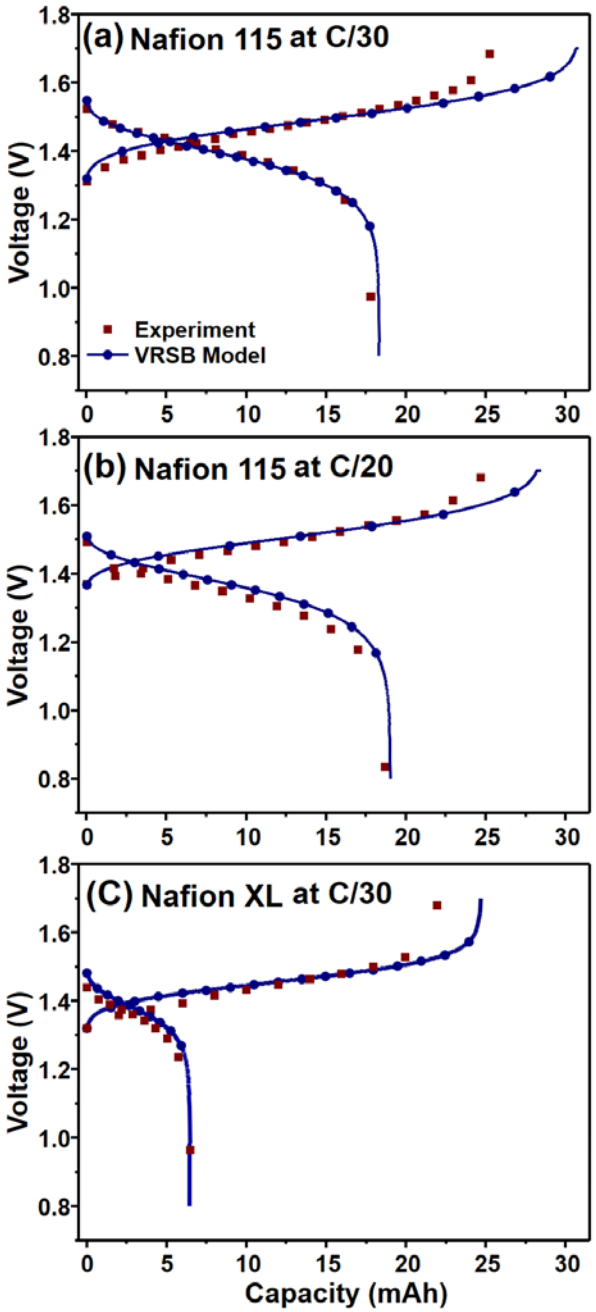

Figure S2. Comparison of voltage profiles between uni-directional model outputs and experimental data from the static cell system. Voltage profiles of Nafion 115 system at (a) C/30 and (b) C/20 and (c) Nafion XL system at C/30 (Experimental data: wine color and filled square dots, VRSB model outputs: blue color and filled circle plot).

Nafion 115 system. The same way to estimate parameters in the main text was used. The reference rate constants and the diffusion distance are expressed in term of an exponential function, and these exponents were used as optimizing variables. Initial guesses and bounds for the diffusion distance, reference rate constants at positive and negative electrodes, the contact resistance, and the formal potential were the same values in the main text. The initial guesses for the potential gradients at C/30 and C/20 were 0.9×10^{-4} and 0.158×10^{-3} V/um, respectively. The bounds for the potential gradient at C/30 and C/20 were given as 0.88×10^{-4} to 0.93×10^{-4} V/um and 0.155×10^{-3} and 0.16×10^{-3} V/um, respectively. The converged parameters for the diffusion distance, the potential gradient at C/30 and C/20, reference rate constants at positive and negative electrodes, the contact resistance, and the formal potential are 129.4120 um, 0.9224×10^{-4} V/um , 0.1575×10^{-3} V/um , 5.0443×10^{-7} m/s, 2.2585×10^{-6} m/s , 13.08136, and 1.4497, respectively. Also, the minimized MSE was 12.389mV.

Nafion XL system. The reference rate constants and the diffusion distance are expressed in term of an exponential function, and these exponents were used as optimizing variables. The initial guesses and bounds for the the diffusion distance and four diffusion coefficients of V^{2+}, V^{3+}, VO^{2+}, and VO_2^{+} are the same values in the main text. The initial guess for the potential gradient was 0.58×10^{-4} V/um. The bound for the potential gradient was given as 0.55×10^{-4} to 0.6×10^{-4} V/um. The converged parameters for the diffusion distance, the potential gradient, and four diffusion coefficients of V^{2+}, V^{3+}, VO^{2+}, and VO_2^{+} are 100.9560 V/um, 0.6259 V/um, 8.1883×10^{-12} m^2/s, 3.9042×10^{-12} m^2/s, 2.4783×10^{-11} m^2/s, and 1.7144×10^{-11} m^2/s, respectively. Also, the minimized error was 1.228 mV.

SM 3. Simulations at other C-rates. The estimated parameters in the previous step were applied to the system at other C-rates (C/10 for the Nafion 115 system and C/20 for the Nafion XL system), except for the potential gradient inside a membrane. The potential gradient was estimated directly at the C-rates. The MSE of the Nafion 115 system at C/10 is 0.9773 mV, and the MSE of the Nafion XL system at C/20 is 6.5638 mV. Also, the estimated potential gradients are 5.0423×10^{-4} V/um and 0.52×10^{-4} V/um at the Nafion 115 system and the Nafion XL system, respectively.

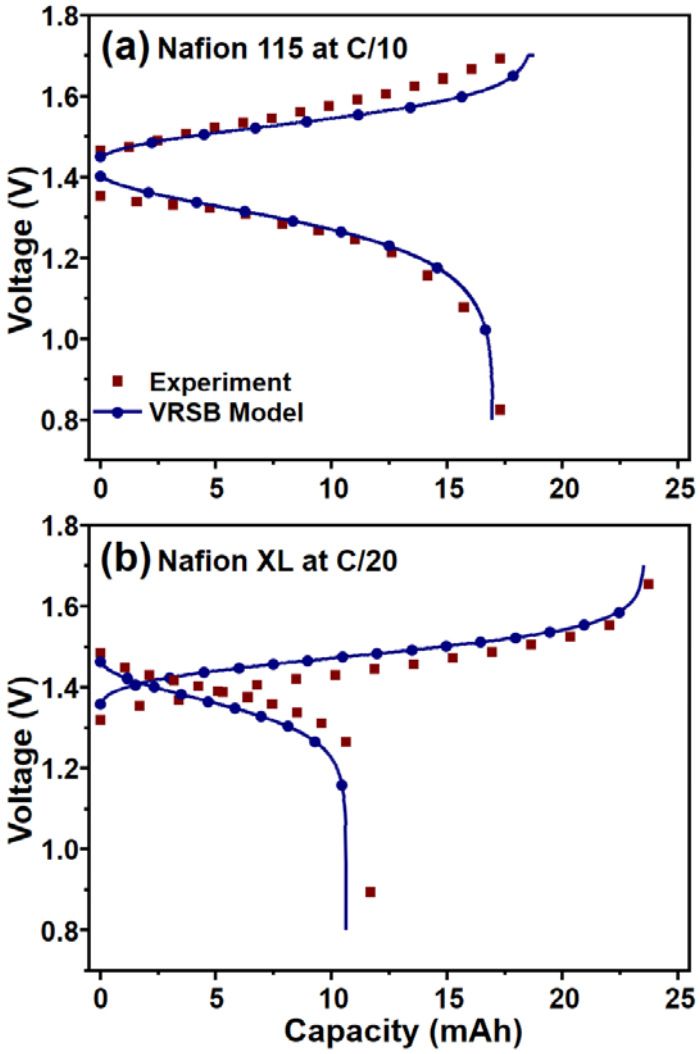

Figure S3. Comparison of voltage profiles between model outputs and experimental data from the static cell system. Voltage profiles at (a) Nafion 115 at C/10 and and (b) Nafion XL at C/20 (Experimental data: wine color and filled square dots, VRSB model outputs: blue color and filled circle plot).

SM 4. Executable program. There are two sets of executables and text files for the Nafion 115 and Nafion XL systems. They are run on any Windows based PC environment. Each set contains an executable file and three text files. Also, open source files will be provided for users' convenience. Users can download DASKR (https://www.xxx) and GA (https://www.xxx) and combine them by themselves. All relevant files can be downloaded directly from the Dr. Subramanian group's website as a zip file (http://depts.washington.edu/maple/xxxx.html). Once download the zip files, unzip all the files into the same folder. Below is the detailed instruction.

The Nafion 115 system. The executable file ('Estimation_Nafion 115 system.exe') in the zip file can estimate six parameters of the Nafion 115 system: the diffusion distance, the reference rate constant at anode and cathode, the contact resistance, the formal potential, and the potential gradient inside a membrane. The executable file uses two sets of CC-CV charging and CC discharging profiles.

1. Identify your experimental conditions. The uploaded executable file utilizes a value of applied current, a regular time interval for each profile, and the number of voltage data. Users can put their own experimental conditions to the Experimental condition text file. The first and second rows represent values of applied currents for CC-charging and CC discharging for Nafion 115 system at two different C-rates. The original text file contains C/20 (0.000893 A) and C/30 (0.00134) for those rows. The third and fourth rows represent time intervals of CC-charging and CC-discharging at C/20, and the fifth and sixth rows represent time intervals of the same at C/30. In the uploaded text file, the time interval was collected at every 338.4703015 and 253.6387437 second for charging and discharging at C/20, and the C/30 operation collected data at every 513.6658291 and 362.4611558 seconds for the same. In the Last row, users need to put the number of the experimental data. In the original file, the number of 200 experimental voltage data was used.
2. Input experimental voltage data at two different C-rates into the Voltage data text file. Note that the same number of experimental data was prepared for 4 different charging and discharging profiles. The first and second columns present voltage data for charging and discharging at C/20, respectively. The third and fourth columns present voltage data for charging and discharging at C/30. Users can input their experimental data sequentially.
3. Input bounds for parameters into the Bound text file. The bounds are given as a 6 by 2 array: the value of the left and right sides present lower and upper bounds, respectively. The bounds are given for the following sequence: the diffusion distance, reference rate constants at anode and cathode, Resistance, the formal potential, and the potential gradients at C/20 and C/30.
4. Double click and run the execution file: 'Estimation_Nafion 115 system.exe'. A command line window will be opened, and the program will calculate the optimal

values of parameters. Once finishing the calculation, the command window will be closed. No action required.

5. The optimization results for all the variables can be found in the "Estimated parameters.csv". The results will be given by the following sequence: the diffusion distance, reference rate constants at anode and cathode, Resistance, the formal potential, and the potential gradient at C/20 and C/30

The Nafion XL system. The second program (Other membrane system.exe) can estimate four vanadium ions' diffusion coefficients of other membranes, the diffusion distance, and the potential gradient inside a membrane. The protocol to execute the executable file is similar to the previous step.

1. Identify your experimental conditions. Users can put their own experimental conditions to the Experimental conditions text file. In the uploaded text file, the first row represents a value of applied currents for CC-charging and CC-discharging for the Nafion XL system at C/30. The second and third rows represent time intervals of CC-charging and CC-discharging. Here, the time interval was collected at every 446.7550251 and 105.1483133 seconds for charging and discharging at C/30. In the fourth row, users need to put the number of the experimental data. In the original file, the number of 200 experimental voltage data was used. From the fifth to the eighth rows, the information obtained in the Nafion 115 system was used. The Fifth and sixth rows represent the reference rate constant at anode and cathode, the seventh row represents the contact resistance, and the eighth row represents the formal potential of the static system.
2. Input bounds for parameters into the Bounds text file. The bounds are given as a 6 by 2 array: the value of the left and right sides present lower and upper bounds, respectively. The bounds are given for the following sequence: the diffusion distance, diffusion coefficients of V^{2+}, V^{3+}, VO^{2+}, and VO_2^{+}, and the potential gradient.
3. Double click and run the execution file: 'Other membrane systems.exe'. A command line window will be opened, and the program will calculate the optimal values of parameters. Once finishing the calculation, the command window will be closed. No action required.
4. The optimization results for all the variables can be found in the "Estimated parameters.csv". The results will be given by the following sequence: the diffusion distance, diffusion coefficients of V^{2+}, V^{3+}, VO^{2+}, and VO_2^{+}, and the potential gradient.

Supporting Tables S1-S2

Table S1. Governing Equations of VRSBs (uni-migration effects)

Accumulation	**= Generation**	**+ In – Out** (Diffusion terms)	(Migration terms)	**No.**
Charge				
$V_r \frac{dC_{V^{2+}}(t)}{dt}$	$= +\frac{j_{app}}{F} A_{elec}$	$-\left(D_{V^{2+}} C_{V^{2+}}(t) + 2D_{VO_2^+} C_{VO_2^+}(t) + D_{VO^{2+}} C_{VO^{2+}}(t)\right)\frac{A_{mem}}{\delta_{diff}}$	$-2\left(D_{VO^{2+}} C_{VO^{2+}}(t) + D_{VO_2^+} C_{VO_2^+}(t)\right)\frac{F}{RT} A_{mem} \nabla\phi$	**[1S]**
$V_r \frac{dC_{V^{3+}}(t)}{dt}$	$= -\frac{j_{app}}{F} A_{elec}$	$-\left(D_{V^{3+}} C_{V^{3+}}(t) - 3D_{VO_2^+} C_{VO_2^+}(t) - 2D_{VO^{2+}} C_{VO^{2+}}(t)\right)\frac{A_{mem}}{\delta_{diff}}$	$+\left(4D_{VO^{2+}} C_{VO^{2+}}(t) + 3D_{VO_2^+} C_{VO_2^+}(t)\right)\frac{F}{RT} A_{mem} \nabla\phi$	**[2S]**
$V_r \frac{dC_{VO^{2+}}(t)}{dt}$	$= -\frac{j_{app}}{F} A_{elec}$	$-\left(D_{VO^{2+}} C_{VO^{2+}}(t) - 3D_{V^{2+}} C_{V^{2+}}(t) - 2D_{V^{3+}} C_{V^{3+}}(t)\right)\frac{A_{mem}}{\delta_{diff}}$	$-2D_{VO^{2+}} C_{VO^{2+}}(t)\frac{F}{RT} A_{mem} \nabla\phi$	**[3S]**
$V_r \frac{dC_{VO_2^+}(t)}{dt}$	$= +\frac{j_{app}}{F} A_{elec}$	$-\left(D_{VO_2^+} C_{VO_2^+}(t) + 2D_{V^{2+}} C_{V^{2+}}(t) + D_{V^{3+}} C_{V^{3+}}(t)\right)\frac{A_{mem}}{\delta_{diff}}$	$-D_{VO_2^+} C_{VO_2^+}(t)\frac{F}{RT} A_{mem} \nabla\phi$	**[4S]**
Discharge				
$V_r \frac{dC_{V^{2+}}(t)}{dt}$	$= +\frac{j_{app}}{F} A_{elec}$	$-\left(D_{V^{2+}} C_{V^{2+}}(t) + 2D_{VO_2^+} C_{VO_2^+}(t) + D_{VO^{2+}} C_{VO^{2+}}(t)\right)\frac{A_{mem}}{\delta_{diff}}$	$-2D_{V^{2+}} C_{V^{2+}}(t)\frac{F}{RT}\frac{\Delta\phi(t)}{\delta_{diff}} A_{mem}$	**[5S]**
$V_r \frac{dC_{V^{3+}}(t)}{dt}$	$= -\frac{j_{app}}{F} A_{elec}$	$-\left(D_{V^{3+}} C_{V^{3+}}(t) - 3D_{VO_2^+} C_{VO_2^+}(t) - 2D_{VO^{2+}} C_{VO^{2+}}(t)\right)\frac{A_{mem}}{\delta_{diff}}$	$-3D_{V^{3+}} C_{V^{3+}}(t)\frac{F}{RT}\frac{\Delta\phi(t)}{\delta_{diff}} A_{mem}$	**[6S]**
$V_r \frac{dC_{VO^{2+}}(t)}{dt}$	$= -\frac{j_{app}}{F} A_{elec}$	$-\left(D_{VO^{2+}} C_{VO^{2+}}(t) - 3D_{V^{2+}} C_{V^{2+}}(t) - 2D_{V^{3+}} C_{V^{3+}}(t)\right)\frac{A_{mem}}{\delta_{diff}}$	$+6\left(D_{V^{2+}} C_{V^{2+}}(t) + D_{V^{3+}} C_{V^{3+}}(t)\right)\frac{F}{RT}\frac{\Delta\phi(t)}{\delta_{diff}} A_{mem}$	**[7S]**
$V_r \frac{dC_{VO_2^+}(t)}{dt}$	$= +\frac{j_{app}}{F} A_{elec}$	$-\left(D_{VO_2^+} C_{VO_2^+}(t) + 2D_{V^{2+}} C_{V^{2+}}(t) + D_{V^{3+}} C_{V^{3+}}(t)\right)\frac{A_{mem}}{\delta_{diff}}$	$-\left(4D_{V^{2+}} C_{V^{2+}}(t) + 3D_{V^{3+}} C_{V^{3+}}(t)\right)\frac{F}{RT}\frac{\Delta\phi(t)}{\delta_{diff}} A_{mem}$	**[8S]**

Table S2. Estimated Parameters of VRSBs (uni-migration effects)

Symbol	Parameter	Lower bound	Upper bound	Initial guess	Final value
$R_{contact}$	Resistance	12	15	13.8104	13.0814 (Ω)
$k_{c,ref}$	Reference rate constant at positive electrode	5.0435×10^{-7}	6.1601×10^{-7}	5.4037×10^{-7}	5.0445×10^{-7} ($m\,s^{-1}$)
$k_{a,ref}$	Reference rate constant at negative electrode	1.8506×10^{-6}	2.2603×10^{-6}	2.2116×10^{-6}	2.2585×10^{-6} ($m\,s^{-1}$)
E_0	Formal potential	1.43	1.45	1.4362	1.4497 (V)
δ_{diff}	Diffusion distance				
	Nafion 115	127	150.7331	136.3889	129.4120 (um)
	Nafion XL	82.7241	102.0549	100	101.9560 (um)
$\nabla\Phi$	Potential gradient				
	Nafion 115 at C/30	0.88×10^{-4}	0.93×10^{-4}	0.90×10^{-4}	0.9224×10^{-4} (V/um)
	At C/20	0.155×10^{-3}	0.160×10^{-3}	0.158×10^{-3}	1.5748×10^{-4} (V/um)
	Nafion XL system	0.59×10^{-4}	0.66×10^{-4}	0.60×10^{-4}	0.6259×10^{-4} (V/um)
$D_{V^{2+}}$	V^{2+} diffusion coefficient for Nafion XL	7.9329×10^{-12}	9.3094×10^{-12}	9.1201×10^{-12}	8.1883×10^{-12} ($m^2\,s^{-1}$)
$D_{V^{3+}}$	V^{3+} diffusion coefficient for Nafion XL	3.0988×10^{-12}	4.1830×10^{-12}	3.9811×10^{-12}	3.9042×10^{-12} ($m^2\,s^{-1}$)
$D_{VO^{2+}}$	VO^{2+} diffusion coefficient for Nafion XL	1.9906×10^{-11}	3.1849×10^{-11}	2.4279×10^{-11}	2.4783×10^{-11} ($m^2\,s^{-1}$)
$D_{VO_2^+}$	VO_2^+ diffusion coefficient for Nafion XL	1.6963×10^{-11}	1.7832×10^{-11}	1.7378×10^{-11}	1.7143×10^{-11} ($m^2\,s^{-1}$)